Journal of Power Sources 190 (2009) 2–13

Contents lists available at ScienceDirect

Journal of Power Sources

journal homepage: www.elsevier.com/locate/jpowsour

Ethanol electrooxidation on a carbon-supported Pt catalyst at elevated temperature and pressure: A high-temperature/high-pressure DEMS study

S. Sun, M. Chojak Halseid[1], M. Heinen, Z. Jusys, R.J. Behm*

Institute of Surface Chemistry and Catalysis, Ulm University, D-89069 Ulm, Germany

ARTICLE INFO

Article history:
Received 26 January 2009
Accepted 26 January 2009
Available online 6 February 2009

Keywords:
Ethanol oxidation
Elevated temperature
Elevated pressure
DEMS
CO_2 current efficiency
Activation energy

ABSTRACT

The electrooxidation of ethanol on a Pt/Vulcan catalyst was investigated in model studies by on-line differential electrochemical mass spectrometry (DEMS) over a wide range of reaction temperatures (23–100 °C). Potentiodynamic and potentiostatic measurements of the Faradaic current and the CO_2 formation rate, performed at 3 bar overpressure under well-defined transport and diffusion conditions reveal significant effects of temperature, potential and ethanol concentration on the total reaction activity and on the selectivity for the pathway toward complete oxidation to CO_2. The latter pathway increasingly prevails at higher temperature, lower concentration and lower potentials (~90% current efficiency for CO_2 formation at 100 °C, 0.01 M, 0.48 V), while at higher ethanol concentrations (0.1 M), higher potentials or lower temperatures the current efficiency for CO_2 formation drops, reaching values of a few percent at room temperature. These trends result in a significantly higher apparent activation barrier for complete oxidation to CO_2 (68 ± 2 kJ mol^{-1} at 0.48 V, 0.1 M) compared to that of the overall ethanol oxidation reaction determined from the Faradaic current (42 ± 2 kJ mol^{-1} at 0.48 V, 0.1 M). The mechanistic implications of these results and the importance of relevant reaction and mass transport conditions in model studies for reaction predictions in fuel cell applications are discussed.

1. Introduction

Direct ethanol fuel cells (DEFCs) have received growing attention as renewable power sources during recent years [1–8]. The successful introduction of DEFCs is hindered, however, by the slow kinetics of the ethanol electrooxidation reaction and its poor selectivity toward complete oxidation to CO_2 [6,9–16], while much or even most of the ethanol is only partly oxidized to acetaldehyde or acetic acid (see below). The kinetics and mechanism of the ethanol oxidation reaction (EOR) have been investigated extensively in model studies on massive electrodes and supported catalysts electrodes, employing purely electrochemical measurements as well as *in situ* spectroscopic techniques (for a summary see below). Direct transfer of these results to the reaction in a realistic fuel cell, however, is hardly possible because of the very different reaction and mass transport conditions in both cases: While DEFCs are operated at elevated temperatures under enforced electrolyte transport, using high surface area electrodes, model studies are mostly performed at room temperature and in stagnant electrolyte, in the absence of enforced electrolyte transport, and often on massive metal electrodes with low surface area (for reviews see [17,18]). Detailed reaction studies performed using realistic fuel cells, on the other hand, are rare [6,9,14,15,19,20], and the reaction conditions are much less defined than those in model studies and may differ significantly between different studies. For instance, measurements of the CO_2 product yield and CO_2 current efficiency, which were performed in three different studies [6,9,19,20], arrived at widely differing results. Measuring the relative product distribution for ethanol oxidation at the exhaust of a polybenzamidazole (PBI) fuel cell by on-line mass spectrometry (temperature range 150–190 °C), Wang et al. determined acetaldehyde as the main reaction product and CO_2 as a minority product, with the CO_2 content increasing with increasing water-to-ethanol ratio [9]. On the other hand, Aricò et al. reported a high selectivity toward CO_2 formation (95%) for ethanol oxidation in a liquid-feed polymer electrolyte fuel cell with a PtRu/Vulcan anode catalyst (145 °C, 1 M ethanol) [19]. Comparable results were published by Rao et al. for ethanol oxidation over a Pt/C catalyst, who measured the CO_2 concentration at the exhaust of a DEFC by on-line mass spectrometry in the temperature range between 30 and 90 °C and obtained a current efficiency for CO_2 formation of more than 75% at 90 °C (0.1 M ethanol, 5 mg cm^{-2} Pt catalyst loading), whereas for 1 M ethanol oxidation on a PtRu/C catalyst MEA the current efficiency for CO_2 formation was significantly lower [20].

Comparable model studies, which were performed at room temperature in stagnant electrolyte, also led to diverging results on the product distribution [11,12,21,22]. Hitmi et al. determined acetic acid as main product for ethanol oxidation on polycrystalline Pt at

* Corresponding author.
E-mail address: juergen.behm@uni-ulm.de (R.J. Behm).
[1] Present address: Institute for Energy Technology (IFE), 2007 Kjeller, Norway.

0378-7753/$ – see front matter © 2009 Elsevier B.V. All rights reserved.
doi:10.1016/j.jpowsour.2009.01.073

10 °C/0.8 V at low concentrations (<0.01 M), whereas acetaldehyde prevailed at high concentration (>0.1 M) [21]. In contrast, much higher relative yields of CO_2, reaching even 100%, were determined by on-line differential electrochemical mass spectrometry (DEMS) for ethanol oxidation on PtRu electrodes at low temperatures (5 and 25 °C) [22]. On the other hand, rather low current efficiencies for CO_2 formation were obtained in model studies over PtRu and PtRu/C catalysts [23–26]. Without commenting on the very different results of these model studies, it is clear that the reaction conditions are incommensurable with those in fuel cell measurements. Recently, Wang et al. systematically investigated the product distribution of ethanol oxidation over a Pt/Vulcan catalyst as a function of temperature (23–60 °C), ethanol concentration and catalyst loading in a model study by DEMS, using a thin-film supported catalyst (Pt/Vulcan) electrode with negligible diffusion resistance and well defined enforced electrolyte mass transport [10]. Incomplete ethanol oxidation to acetaldehyde and acetic acid was found to prevail over complete oxidation to CO_2 under these experimental conditions, with CO_2 current efficiencies in the range of a few percent at most.

To further approach the situation in a realistic fuel cell, while maintaining the well defined reaction and transport conditions in model studies, it is particularly important to raise the reaction temperature to at least 100 °C, possibly even higher, which also requires pressurizing the reaction cell and the electrolyte to prevent evaporation of electrolyte and reactants. A number of groups reported the build-up of pressurized high-temperature cells [27–37]. These cells allow operation at relevant temperatures, mostly also under controlled and enforced electrolyte transport, but are limited to purely electrochemical measurements.

Recently, we developed a high-temperature/high-pressure DEMS set-up which allows electrocatalytic measurements on supported catalyst thin-film electrodes (ca. 100% catalyst utilization, negligible diffusion limitations) at elevated temperatures (up to 100 °C) and pressure (3 bar overpressure) under continuous reaction and well defined, enforced mass transport conditions [38]. This set-up was employed to investigate the electrooxidation of ethanol on carbon supported Pt/Vulcan catalysts at temperatures up to 100 °C under well defined and fuel cell relevant reaction and transport conditions. Although from experimental reasons we can not discriminate between acetaldehyde and acetic acid product formation at present (see Section 2), this allows us to discriminate between partial oxidation (acetaldehyde, acetic acid formation) and complete oxidation (CO_2 formation), which is particularly interesting for practical applications. Preliminary results of this study were published recently [38].

In the following we will, after a brief description of the experimental set-up and procedures (Section 2), first present and discuss results of potentiodynamic (Section 3.1) and potentiostatic (Section 3.2) measurements in 0.1 M and 0.01 M ethanol solutions, covering the wide temperature range between ambient temperature and 100 °C. The data are used to evaluate the current efficiency for the complete oxidation of ethanol to CO_2 under different conditions, and to calculate the apparent activation energies for the overall ethanol oxidation and for complete oxidation to CO_2 at different potentials (Section 3.3). Finally, the mechanistic and kinetic implications arising from these data as well as the importance of realistic reaction conditions in model studies for the prediction of the reaction behavior in fuel cells will be discussed.

2. Experimental

2.1. Elevated temperature DEMS set-up and experimental details

The DEMS set-up consists of the actual DEMS flow cell assembly, a differentially pumped two-chamber ultrahigh vacuum (UHV) system with a Balzers QMS 112 quadrupole mass spectrometer, a Pine Instruments potentiostat (model AFRDE5) and a computerized data acquisition system and had been described in more detail previously [38,39].

The DEMS flow cell assembly consisted of an electrochemical thin-layer flow cell, which was placed in a home-built air thermostat, and a second thin-layer compartment, which was connected to the electrochemical cell by an inert capillary and to the UHV system containing the mass spectrometer. A thin Teflon membrane (10 μm thick), supported on a stainless steel frit, separated the second compartment from the UHV. The electrolyte was supplied from pressurized glass bottles thermostated separately in two commercial thermostats (Lauda E200), the electrolyte flow was controlled by a pressure-resistant syringe pump (Harward Apparatus 11 plus) connected to the outlet of the second flow compartment. The time delay between the onset in the production of gaseous species and their mass spectrometric detection (~4 s at a flow rate of 15 μL s^{-1}), caused by the finite time required for the electrolyte to flow from the first to the second (detector) compartment, was corrected for accordingly.

The electrochemical thin-layer channel flow cell had been described and characterized in terms of its mass transport recently [35,38]. A Pt wire serving as counter electrode was placed in a separate compartment in the cell body, behind a glass frit in a circular opening directly in front of the working electrode. An external saturated calomel electrode (SCE), kept at ambient temperature, was used as a reference. All potentials, however, are quoted against that of a reversible hydrogen electrode (RHE). The potential with respect to the saturated calomel electrode was corrected to that of a reversible hydrogen electrode (RHE) reference at the respective reaction temperatures by measuring the onset of the HOR/HER on the same Pt/Vulcan catalyst thin film electrode at various temperatures under a constant hydrogen overpressure of 3 bar.

The circular thin-film Pt/Vulcan (20 wt% metal, E-TEK Inc.) electrode was prepared following the procedure described in ref. [40], by pipetting and drying 20 μL of an ultrasonically re-dispersed aqueous catalyst suspension (2 mg mL^{-1}) and then 20 μL of aqueous Nafion solution in the center of the mirror-polished planar glassy carbon rectangular plate (Sigradur G from Hochtemperatur Werkstoffe GmbH, 30 mm × 20 mm × 6 mm). This plate was mounted on the flow cell body. The resulting thin catalyst film had a diameter of ca. 5 mm, a geometric surface area of 0.2 cm^2, and a Pt loading of 40 μg_{Pt} cm^{-2}.

Before each measurement, the cell was carefully flushed with supporting electrolyte, then the thin-film electrode was cycled in the potential range between 0.06 and 1.16 V (100 mV s^{-1} scan rate), until the cyclic voltammogram of a clean Pt/C electrode was reproduced [39]. The H_{upd} charge was used as an inherent reference to check for possible losses of catalyst after each experiment.

The supporting electrolyte was prepared using Millipore MilliQ water and suprapure sulfuric acid (Merck, suprapur). Ethanol (LiChrosolv) and formic acid (GR) were obtained from Merck. Before the measurements, all solutions were deaerated by high-purity Ar (MTI Gase, N6.0). All experiments were carried out at an overpressure of 3 bar and at temperatures between 23 and 100 °C, as indicated.

2.2. Calibration of elevated temperature and pressure DEMS set-up

The use of a non-porous Teflon membrane with low permeability, which was required to keep the water vapor level at tolerable levels at high temperatures and elevated pressure, also inhibits the permeation of larger molecules such as acetaldehyde. This allows us to monitor the CO_2 partial pressure via the $m/z = 44$ signal, without interference with the acetaldehyde signal at $m/z = 44$. The

absence of acetaldehyde vapor in the mass spectrometer chamber was confirmed by featureless signals of the $m/z = 29$ ion current (CHO^+ fragment of acetaldehyde) as a function of the potential. Furthermore, we found no change in the background level at $m/z = 44$ when changing from supporting electrolyte to a pressurized (3 bar overpressure) 0.01 M acetaldehyde solution at all temperatures. Furthermore, the ion current at $m/z = 22$ (doubly ionized CO_2^{2+}, 2.8% of the main $m/z = 44$ CO_2 peak [10]), which was also recorded in all experiments, was found to quantitatively agree with the $m/z = 44$ signal. Therefore, in Section 3, we will only show the $m/z = 44$ signal, because of its much better signal-to-noise ratio.

The partial current for complete ethanol electrooxidation to CO_2, $I_F(CO_2)$, was calculated using the following equation:

$$I_F(CO_2) = \frac{6 I_{MS}(m/z = 44)}{K^*_{44}} \quad (2)$$

where I_{MS} ($m/z = 44$) is the mass spectrometric current of the $m/z = 44$ signal, the factor of 6 reflects the average number of electrons needed for formation of one CO_2 molecule per C atom in ethanol, and K^*_{44} is the calibration constant for $m/z = 44$, determined by potentiostatic HCOOH bulk oxidation at the respective temperatures, from 23 to 100 °C, on a Pt/Vulcan catalyst. K^*_{44} was calculated by

$$K^*_{44} = \frac{2 I_{MS}(m/z = 44)}{I_F} \quad (3)$$

where I_F is the Faradaic current during HCOOH bulk oxidation, and I_{MS} ($m/z = 44$) is the corresponding mass spectrometric current of the $m/z = 44$ signal, 2 is the number of electrons needed for formation of one CO_2 molecule from HCOOH. To remove effects from the temperature dependence on the permeability of the membrane, the CO_2 related $m/z = 44$ signals are normalized to the K^* value at room temperature determined as reference before each series of measurements.

The current efficiency for CO_2 formation was calculated as the ratio of the partial current for ethanol oxidation to CO_2 (see Eq. (2)), $I_F(CO_2)$, and the overall Faradaic current for ethanol oxidation.

The apparent activation energies for ethanol oxidation to CO_2 and for the overall oxidation reaction were calculated from the slopes in the Arrhenius plots of the partial currents for ethanol oxidation to CO_2, $I_F(CO_2)$, and the total Faradaic currents, respectively, at steady-state during constant potential ethanol oxidation.

3. Results and discussion

3.1. Potentiodynamic oxidation of ethanol on a Pt/Vulcan catalyst at elevated temperatures

Fig. 1 shows a series of potentiodynamic DEMS measurements of the ethanol electrooxidation reaction over the Pt/Vulcan catalyst in 0.1 M ethanol containing 0.5 M H_2SO_4 solution at different temperatures (23, 40, 50, 60, 70, 80, 90 and 100 °C). (Note that the Faradaic current was corrected for pseudo-capacitive contributions due to double-layer charging). The top panels depict the Faradaic current traces (Fig. 1a and d), the $m/z = 44$ mass spectrometric ion current signals are shown in the central panels (Fig. 1b and e). Finally, the bottom panels depict the current efficiencies for CO_2 formation calculated from the above data (Fig. 1c and f). For more clarity, the forward-going scans and the negative-going scans are displayed in two separate panels, with the positive-going scans in the left set of panels (Fig. 1a–c) and the negative-going scan in the right set of panels (Fig. 1d–f). Furthermore, the traces recorded at room temperature are also shown with higher magnification to better identify the shape (for magnifications see figures). Furthermore, the onset

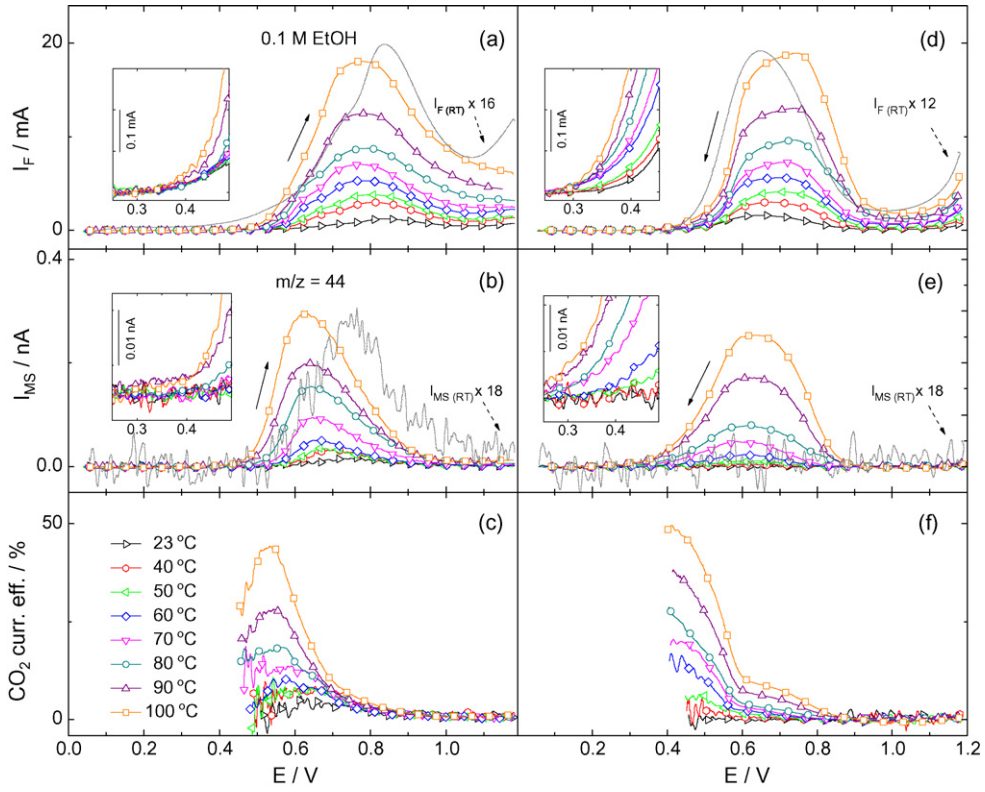

Fig. 1. Simultaneously recorded positive-going scan (a and b) and negative-going scan (d and e) of CVs (a and d) and MSCVs for $m/z = 44$ (b and d), and the corresponding CO_2 current efficiency (c and f) of the ethanol oxidation reaction on a Pt/Vulcan catalyst in 0.1 M ethanol solution pressurized with 3 bar Ar overpressure at elevated temperatures (temperatures see figure). Dashed lines: magnified presentation of the room temperature traces (magnification factors see figure). *Inset*: Magnified presentation of the reaction onset. Arrows indicate the direction of the potential scan. Potential scan rate 10 mV s^{-1}, catalyst loading 40 μg_{Pt} cm^{-2}, electrolyte flow rate 15 $\mu L\, s^{-1}$.

behavior of the Faradaic and mass spectrometric currents is shown in insets with an expanded current scale.

The Faradaic currents at lower temperatures, up to 60 °C, largely resemble those obtained in previous measurements, when accounting for the different reaction and transport conditions [10]. They were discussed in detail in ref. [10], therefore they will only be shortly summarized here. At potentials below about 0.35 V (23 °C) (see inset), the electrooxidation of ethanol is essentially inhibited, which was explained by the presence of a reaction inhibiting ('poisoning') adlayer of adsorbed intermediates, mainly CO_{ad} and smaller amounts of adsorbed hydrocarbon residues (on a bare catalyst surface, at low H_{upd} and CO_{ad} coverages, ethanol was found to adsorb dissociatively, producing CO_{ad} and $CH_{x,ad}$ species [10,41]). After the reaction onset, the current increases and passes through a broad peak, which consists of two hardly resolved states, a shoulder at ~0.7 V (at 23 °C) and the peak maximum at 0.83 V (at 23 °C, see magnified current trace). By comparison with the ethanol adsorbate stripping behavior, the onset of the reaction is associated with the onset of ethanol adsorbate oxidation, which lowers the adsorbate coverage and allows increasing OH_{ad} formation and their reaction with EOR reaction intermediates [10]. At higher potentials (>0.83 V), the ethanol oxidation rate decreases, which is commonly assigned to an increasing OH_{ad} coverage/surface oxide formation on the Pt electrode [17], and reaches a plateau at 1.0 V. Even at potentials >1.0 V, ethanol oxidation continues at a low, but measurable rate up to the positive potential limit of 1.16 V. In order to avoid possible electrooxidation of the carbon support, the upper potential limit was set to below 1.2 V.

With increasing temperature, the onset potentials shift to slightly lower values, reaching ~0.3 V at 100 °C. The low-potential shoulder visible at 0.7 V at 23 °C also shifts to lower potentials (~0.6 V at 100 °C) and increases in intensity relatively to the main peak, such that at 100 °C it forms a broad peak together with the previous main maximum and cannot be resolved any more. Its further presence will become evident, however, in the CO_2 current efficiency (see below). The main maximum of the peak, finally, shifts from 0.85 V at 23 °C to 0.75 V at 100 °C respectively, following the trends known from previous model studies up to 60 °C [10]. The smooth current decrease at the high-potential side of the peak extends to increasingly more positive values, reaching up to the positive potential limit of 1.16 V at 100 °C. The maximum Faradaic current for ethanol oxidation increases considerably, by a factor of ca. 14, in the temperature range from 23 to 100 °C. The downshift of the onset potential and in particular of the peak maxima with increasing temperature is related to the thermal activation of the ethanol adsorbate oxidation process and of the OH_{ad} formation process (see also ref. [29,42,43]). Similar shifts were observed also in earlier temperature dependent studies of methanol oxidation on Pt and PtRu alloy electrodes, and attributed to an increasing thermal activation of water splitting [34,44–46]. Finally, also the high-potential current at potentials positive of 1.0 V increases significantly with temperature.

The $m/z = 44$ ion current signals largely follow the Faradaic current signals after correcting for the time delay between Faradaic current measurement and mass spectrometric measurement (time constant of the flow cell, ~4 s). CO_2 formation starts at 0.4 V at room temperature in the positive-going scan (see inset). After passing through a maximum at 0.73 V (23 °C), it decreases again and reaches the base line at 1.0 V. Compared to the Faradaic current signal, the peak is less broad, and mainly consists of a single state, which coincides with the low-potential state in the Faradaic current [10,25]. In a previous study, it was demonstrated that this peak is at least partly due to oxidation of adsorbed species ('ethanol adsorbate'), that had been formed at lower potentials in the preceding negative-going scan, mainly CO_{ad} and $CH_{x,ad}$ [25,41]. At potentials positive of 1.0 V, the CO_2 formation rate drops to values below the detection limit (23 °C), in contrast to the finite value of the Faradaic current at the potentials positive of 1.0 V. Therefore, the Faradaic current detected at potentials positive of 1.0 V must be related to incomplete oxidation of ethanol (formation of acetaldehyde and acetic acid) and/or Pt surface oxidation. Acetaldehyde formation was in fact detected previously up to 60 °C when using a porous membrane [10]. With increasing temperature, both the onset potential for CO_2 formation and the potential of the peak maximum shift to lower potential, reaching 0.3 and 0.63 V at 100 °C, respectively.

The corresponding current efficiencies for CO_2 formation, which were calculated as described before in Section 2.2, are plotted in Fig. 1c. (The calculations were cut off at potentials where the Faradaic current is <1% of its maximum value, because of the large errors resulting from even small deviations in the current measurement, as they can be introduced, e.g., by the double layer charge correction.) The current efficiencies are dominated by an initial increase with increasing potential, a maximum in the range 0.57–0.67 V, and a subsequent decay, reaching very low values at 1.0 V. With increasing temperature, the CO_2 current efficiency increases steadily, reaching a value of ~45% at the maximum at 100 °C. At temperatures of 60 °C and below, the maximum CO_2 current efficiencies are below 5%. The potential of the maximum decreases with increasing temperature, from 0.6 V at 60 °C to 0.52 V at 100 °C.

Comparing it with the CO_2 ion current signal, the maximum of the CO_2 current efficiency shifts more and more towards the onset of the CO_2 ion current signal. This agrees with the interpretation that the CO_2 formed at the onset of the CO_2 peak results mainly from the oxidation of ethanol adsorbates formed at lower potentials and in the preceding negative-going scan (see above). At room temperature, ethanol adsorbate oxidation even dominates the overall CO_2 formation. With increasing temperature, thermal activation results in an earlier onset of this reaction (cf. also with the downshift in the onset of CO_{ad} oxidation with increasing temperature [43]). This leads to vacant surface sites already at rather low potentials, where C—C bond breaking is more facile [47–50], and allows further CO_{ad} formation and oxidation to CO_2, until C—C bond breaking ceases. In parallel, the EOR proceeds increasingly via incomplete oxidation to C_2 molecules (acetaldehyde and acetic acid). This interpretation agrees fully with our above statement that the Faradaic current peak consists of two states, a low-potential state with a higher contribution from CO_2 formation and a high-potential state where the formation of incompletely oxidized C_2 species prevails [41,51]. It should be noted that due to the contributions from the oxidation of pre-formed ethanol adsorbates, which provides only 2 electrons per CO_2 molecule rather than the 6 electrons assumed in the calculation (complete oxidation of ethanol to CO_2), the real values of the CO_2 current efficiency are lower than the maximum values in Fig. 1c.

The results quantitatively confirm that the current efficiency for CO_2 formation depends strongly on the electrode potential, in agreement with previous findings of DEMS [10,20] and FTIR spectroscopy [52,53] measurements on ethanol oxidation. Furthermore, it is important for realistic fuel cell applications that the overpotential for complete oxidation of ethanol to CO_2 decreases with increasing temperatures.

The negative-going Faradaic current scans resemble the positive-going scans in their general appearance, but exhibit distinct differences in details (Fig. 1d). At high potentials, the Faradaic currents first decrease and pass through a distinct minimum at ~1.0 V before increasing again, in contrast to the steady decrease with potential in this range in the positive-going scans. Furthermore, the Faradaic current peaks exhibit distinct double-peak characteristics, at least at higher temperatures ≥60 °C. At low temperatures, only a single peak is resolved, which is centered at ca. 0.62 V at room temperature. With increasing temperature, two

states develop, at 100 °C the corresponding current maxima are located at about 0.65 and 0.75 V. With decreasing potential, the Faradaic current decreases and reaches the zero level at about 0.3 V (see inset). At the respective peak potentials the Faradaic current increases by a factor of 10 when going from room temperature to 100 °C.

CO_2 formation is completely suppressed over the entire potential range at temperatures below 40 °C (see the magnified current trace), in agreement with findings in a previous DEMS study at room temperature [10,25]. This was explained by the absence of preformed CO_{ad} in the negative-going scan, in combination with an effective inhibition of C–C bond breaking at potentials sufficiently high for CO_{ad} oxidation. At temperatures above 40 °C, CO_2 formation is also observed in the negative-going scan, and increases steadily with increasing temperature. Since CO_{ad} oxidation is fast under these conditions (>0.7 V), the increasing rate of CO_2 formation in the negative-going scan directly reflects the increasing activation of C–C bond breaking (and fast subsequent oxidation to CO_2) under these conditions. Independent of the temperature (at ≥40 °C), it starts at ~0.9 V, passes through a broad maximum at ~0.57 V, and then decreases again to reach the baseline at ~0.2 V.

The observation of CO_2 at potentials where Faradaic currents are not detected, between 0.2 and 0.3 V, results from the finite decay time of the CO_2 signal: Time–response measurements performed for potential step oxidation of formic acid showed that after stepping from 1.0 to 0.06 V it takes about 10 s to reduce the CO_2 signal to 10% of its initial intensity, and about 25 s to decrease to the baseline. Therefore, the decrease of the CO_2 formation rates during ethanol oxidation at potentials below the peak maximum is more rapid than indicated by the mass measured data. In general, similar effects occur also in the positive-going scan, but in this case the CO_2 current decay is slower, and therefore these distortions contribute less.

Finally, the current efficiency for CO_2 formation was calculated in the same way as described above. Again, we obtain a steady increase coming from high potentials, and distinct peaks at potentials between 0.45 V at room temperature and 0.4 V at 100 °C. The related CO_2 current efficiencies in the maxima are between 2.7% at 40 °C and ~50% at 100 °C (CO_2 formation is below the detection limit at temperatures up to 40 °C). In this case, distortions due to oxidation of pre-formed ethanol adsorbates, mainly CO_{ad}, can be ruled out since at the high potentials CO_{ad} is rapidly oxidized once formed. However, at lower potentials, in the potential range of the rapidly decaying CO_2 ion current, the finite decay time of the CO_2 signal described above will result in too high values of the CO_2 current efficiency. Therefore, also for the negative-going scan the real maximum CO_2 current efficiencies will be significantly lower than those displayed in Fig. 1f. (In the positive-going scans such effects are negligible in the potential range of the maximum CO_2 current efficiency). The general tendencies of an increasing CO_2 current efficiency with temperature and a decreasing CO_2 current efficiency with increasing potential at potentials positive of the maximum will not be affected by these effects. The rapidly increasing CO_2 current efficiency in the potential range between 0.6 and 0.45 V reflects the increasing activity for C–C bond breaking at these potentials. This will be discussed and compared with previous findings in more detail in Section 3.2, together with the steady-state ethanol oxidation data.

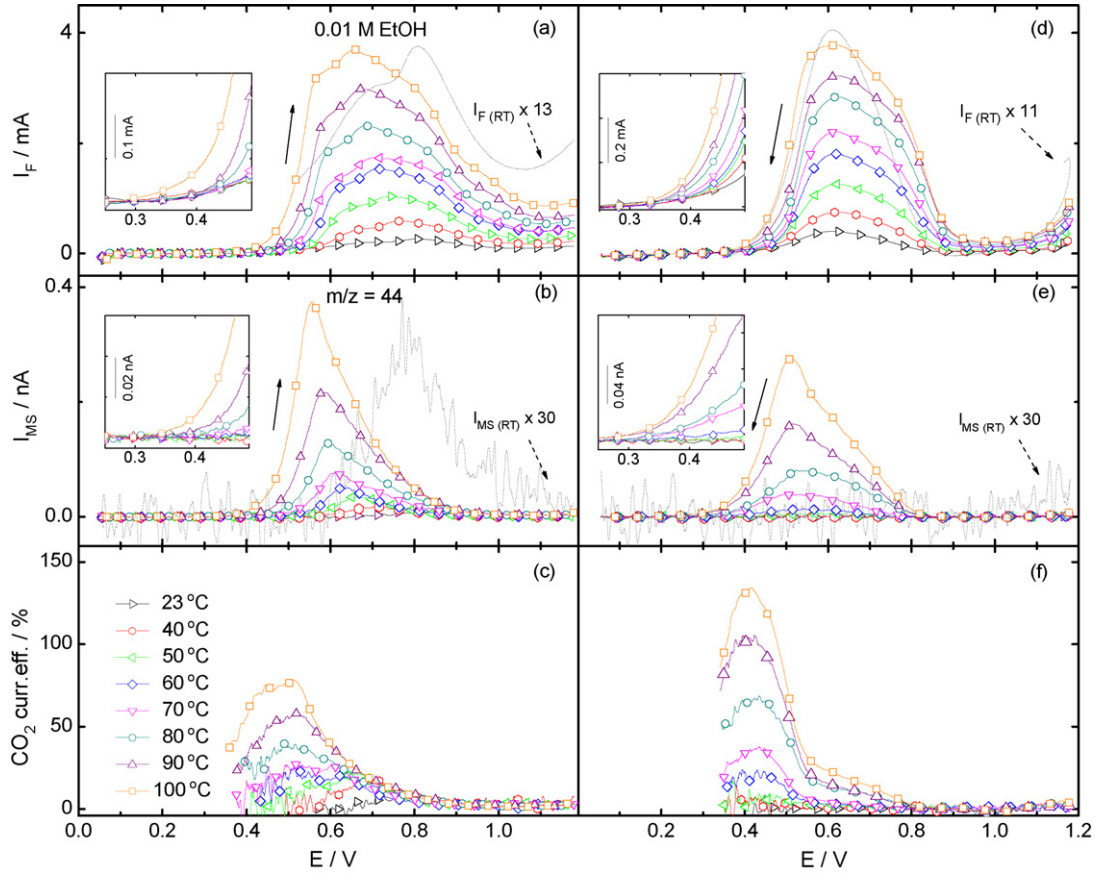

Fig. 2. Simultaneously recorded positive-going scan (a and b) and negative-going scan (d and e) of CVs (a and d) and MSCVs for $m/z = 44$ (b and d), and the corresponding CO_2 current efficiency (c, f) of the ethanol oxidation reaction on a Pt/Vulcan catalyst in 0.01 M ethanol solution pressurized with 3 bar Ar overpressure at elevated temperatures (temperatures see figure). Dashed lines: Magnified presentation of the room temperature traces (magnification factors see figure). *Inset*: Magnified presentation of the reaction onset. Arrows indicate the direction of the potential scan. Potential scan rate 10 mV s^{-1}, catalyst loading 40 μg_{Pt} cm^{-2}, electrolyte flow rate 15 $\mu L\,s^{-1}$.

It is interesting to note that with increasing temperature the peaks in the positive-going and negative-going scan become more and more similar, both for the Faradaic current and the CO_2 ion current. This can be understood from the rapidly increasing reaction rate for CO_2 formation, which reduces the influence of the ethanol adsorbate layer on the reaction behavior more and more. It is oxidatively removed at increasingly lower potentials (pre-formed adsorbate layer in the positive-going scan) or can still be removed at potentials where C–C bond breaking and $C_{1,ad}$ fragment formation are active (negative-going scan). At room temperature, CO_2 formation in the positive-going scan is essentially fully due to oxidation of CO_{ad} pre-formed at lower potentials in the preceding negative-going scan, and in the negative-going scan CO_2 formation is inhibited. With increasing temperature, the pre-formed CO_{ad} can be oxidized at increasingly lower potential, allowing subsequent bulk oxidation to CO_2 via C–C bond breaking and subsequent oxidation of the resulting $C_{1,ad}$ species in the positive-going scan, and this contributes increasingly more to the CO_2 formation charge in the CO_2 ion current peak. In the negative-going scan, C—C bond breaking can occur at potentials where subsequent oxidation of the resulting fragments is still possible, and the latter reaction extends to lower potentials, where C—C bond breaking is increasingly active, until the surface is saturated with adsorbed $C_{1,ad}$ fragments again. Since at more positive potentials the $C_{1,ad}$ coverage is zero, the CO_2 ion current peak fully reflects the rate for C—C bond breaking, except for low potentials, where the resulting $C_{1,ad}$ species are accumulated.

In order to evaluate the influence of the ethanol concentration on the activity and on the current efficiencies for complete ethanol oxidation to CO_2, we performed a similar series of cyclic voltammetry DEMS measurements at lower ethanol concentration (0.01 M) on the same Pt/Vulcan catalyst.

The positive-going (Fig. 2a) and negative-going (Fig. 2d) scans of the cyclic voltammogram for ethanol oxidation in 0.01 M solution closely resemble those obtained in 0.1 M solution (Fig. 1a–f) in their general appearance. Main differences compared to the higher concentration are: (i) The Faradaic current peak at 100 °C is about 1/5 of that in 0.1 M solution in both scan directions, (ii) the onset potential for ethanol oxidation in the positive-going scan is shifted to higher potentials (see insets in Figs. 1a and 2a), (iii) the low-potential peak in the positive-going scan is more pronounced and centered at 0.67 (23 °C)–0.56 V (100 °C). Also, the CO_2 formation curves (Fig. 2b and e) largely resemble those in 0.1 M solution. Different than expected, the absolute currents are of comparable order of magnitude as in 0.1 M solution. Together with the significantly lower Faradaic currents in this case, this points already at higher current efficiencies in 0.01 M ethanol solution than in 0.1 M solution. This is confirmed by the CO_2 current efficiency curves in Fig. 2c and f. The CO_2 formation exhibits a potential dependence which resembles that obtained during 0.1 M ethanol oxidation. The absolute values, however, are significantly higher than in the latter case, with maximum values between 4% at 23 °C and 78% at 100 °C in the positive-going scan, and between below 7% at 40 °C and formally above 100% at 100 °C in the negative-going scan (see later discussion).

These results for lower ethanol concentrations fit well to trends determined in a previous study, where we observed higher relative CO_2 yields, relative to the formation of incomplete oxidation products, for oxidation of 0.01 M ethanol solution compared to 0.1 M ethanol oxidation [10]. Because of the relatively higher contribution from the oxidation of pre-formed ethanol adsorbate in the positive-going scan – the ethanol adsorption rate will be lower for lower ethanol concentrations – and because of the steeper decrease of the CO_2 formation current at potentials cathodic of the maximum in the negative-going scan, the differences between the actual (lower) maximum CO_2 current efficiencies and the measured values will be more pronounced than for reaction in 0.1 M solution. The general trend of an increasing CO_2 current efficiency with decreasing ethanol concentration and otherwise similar reaction conditions, however, resembles the behavior observed under steady-state conditions, in the potentiostatic measurements (see next section), and can therefore be considered as correct.

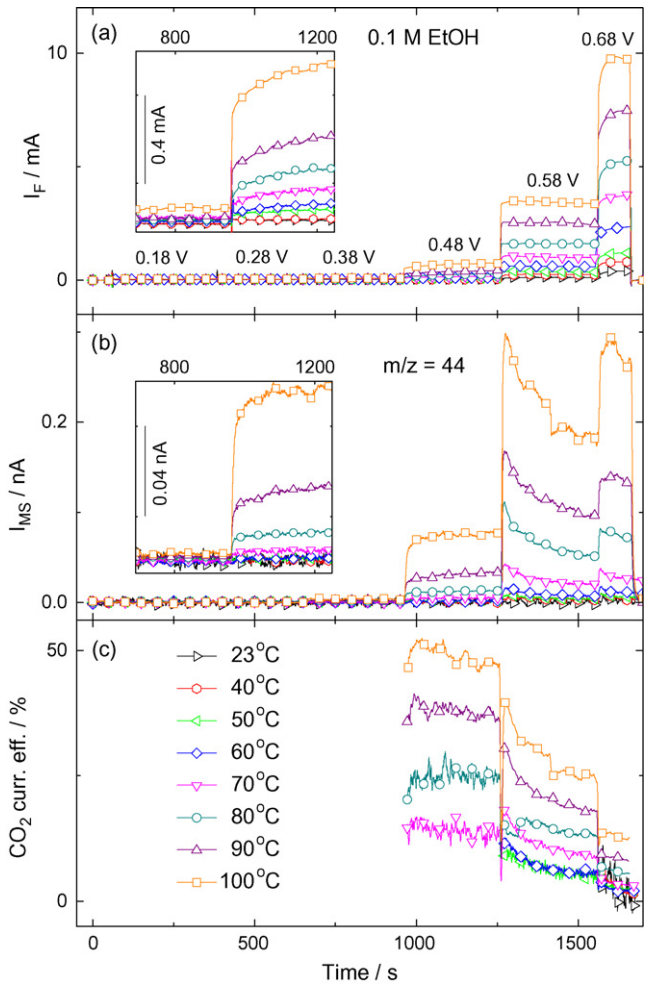

Fig. 3. Simultaneously recorded transients of the Faradaic current (a) and the CO_2 ion currents for $m/z = 44$ (b), and the corresponding current efficiency for CO_2 formation (c) during potentiostatic oxidation of ethanol on a Pt/Vulcan catalyst in 0.1 M ethanol solution pressurized with 3 bar Ar overpressure at elevated temperatures (temperatures see figure). Catalyst loading 40 μg_{Pt} cm^{-2}, electrolyte flow rate 15 $\mu L\,s^{-1}$.

3.2. Potentiostatic oxidation of ethanol on Pt/Vulcan catalyst

More direct information on the ethanol oxidation kinetics and on the effect of the reaction potential is obtained from potentiostatic experiments, where potential and time effects are not convoluted. These also allow us to quantitatively determine the current efficiency for complete ethanol oxidation to CO_2 under steady-state conditions, where the experimental problems encountered in the determination of the CO_2 current efficiency in potentiodynamic measurements are absent. Similarly to the potentiodynamic measurements, we followed the Faradaic current transients (Fig. 3a) and the mass spectrometric ion current transients for CO_2 formation (Fig. 3b, $m/z = 44$) at constant electrode potentials and different reaction temperatures, and calculated the corresponding CO_2 current efficiencies from these data (Fig. 3c). Prior to the constant potential measurements, the negative-going potential scan was stopped at 0.06 V, and held there for 5 min. Therefore, the catalysts are partly covered by adsorbates at the beginning of the

experiment, which is close to the situation expected at the lowest reaction potential (0.18 V). Subsequently, the potential was stepwise increased, first to 0.18 V, and then in increments of 0.1 V to higher potentials. Each potential was held for 5 min, except for the highest potential of 0.68 V, because of the onset of bubble formation. Finally, the potential was stepped back to 0.06 V, holding at this potential until the background signal of the $m/z = 44$ ion current was sufficiently stable for proper background drift correction.

At potentials of 0.28 V and below, the Faradaic current (Fig. 3a) and the mass spectrometric ion current ($m/z = 44$) (Fig. 3b) are below the detection limit, which is attributed to the reaction inhibiting effect of the stable adlayer present on the catalyst under these conditions. This result agrees well with our findings in the potentiodynamic measurements, where the onset of ethanol oxidation occurred at ~0.3 V at 100 °C and slightly more positive at lower temperatures (~0.35 V at 23 °C). Measurable Faradaic currents and mass spectrometric CO_2 signals were detected at 0.38 V at higher temperatures (≥90 °C, see insets in Fig. 3a and b), and at 0.48 V at all temperatures. From 0.48 to 0.58 V and from 0.58 to 0.68 V, the Faradaic current increased by factors of 4.5 and 3, respectively. At 0.48 V, the Faradaic ethanol oxidation current still increases after the potential step, reaching a stable value after ~100 s. At higher potentials, the new Faradaic current values were reached almost instantaneously after each potential step, and the current remained stable at the respective value. The mass spectrometric CO_2 signals also increased with potential, but the increase was less pronounced, and for 0.68 V, the CO_2 signal was almost similar to that obtained at 0.58 V. Furthermore, at both 0.58 and 0.68 V, the CO_2 signal passed through a pronounced initial maximum and then decayed with time to approach the steady-state value. Note that after 300 s this was not yet fully reached. The initial maximum in the CO_2 ion current signal arises from the fast oxidation of part of the CO adlayer present under steady-state conditions at the former potential to CO_2, while at later stages, CO_2 formation is limited to the steady-state CO_{ad} formation rate. The fact that this initial maximum in the CO_2 formation rate is absent in the Faradaic current indicates that with time incomplete oxidation of ethanol increases (at constant potential), compensating for the drop in partial reaction current for CO_2 formation. This increase of the rate for incomplete oxidation product formation has to be significant, considering the much lower electron yield (2–4 electrons compared to 12 electrons per ethanol molecule). At all potentials, both the Faradaic current and the mass spectrometric CO_2 signal increased with temperature, as expected (see Section 3.3). Above 70 °C, the CO_2 formation increased steeply, by factors between 9 and 15 from 70 to 100 °C, depending on the potential.

The current efficiencies for CO_2 formation calculated from these data as discussed in Section 2 are plotted in Fig. 3c and listed in Table 1. They show a clear tendency to (i) decrease with increasing potential and (ii) increase with increasing temperature. At 0.38 V, values of 18 and 23% were calculated for temperatures of 90 °C and 100 °C, respectively. At 0.48 V, they increase from 4.6% at 23 °C to 45% at 100 °C, for 0.58 V and 0.68 V the corresponding ranges of the CO_2 current efficiencies are 3.2–25.7 (23–100 °C) and 1.6–12.6% (23–100 °C), respectively. The increasing probability for CO_2 formation at elevated temperatures, in particular at temperatures of 60 °C and above, agrees well with the findings in the potentiodynamic measurements in Section 3.1. It indicates an increasing activation for C—C bond breaking. Furthermore, this and the equally increasing Faradaic currents demonstrate that also the resulting adsorbed C_1 reaction intermediates are rapidly removed. Apparently, the oxidation of the C–OH group, which results in the reaction by-products acetaldehyde and acetic acid, is much less activated (lower increase with temperature) than C—C bond breaking and $CO_{ad}/CH_{x,ad}$ oxidation (for further discussion see Section 3.3).

Table 1
Steady-state current efficiency for CO_2 formation (in percent) during constant potential ethanol oxidation at different concentrations, potentials and temperatures.

T/°C	0.1 M EtOH			0.01 M EtOH		
	0.48 V	0.58 V	0.68 V	0.48 V	0.58 V	0.68 V
23	4.6	3.2	1.6	5.1	3.7	1.7
40	5.8	4.6	2.3	7.3	5.2	2.6
50	7.8	6.2	2.5	13.8	9.6	3.7
60	9.8	8.0	2.9	26.8	12.9	4.4
70	14.8	10.3	3.9	46.3	17.5	5.3
80	25.7	13.5	6.2	62.1	21.2	8.6
90	36.5	20.1	9.1	75.1	26.1	12.5
100	45.0	25.7	12.6	86.9	31.6	16.6

Comparing the steady-state CO_2 current efficiencies with those obtained in the potentiodynamic measurements (Fig. 1c and f), we find the steady-state values to be in between those in the positive-going and negative-going scans. For instance, at 0.58 V reaction potential, values of about 26% (positive-going scan, negative-going scan: 10%) and 32% (positive-going scan, negative-going scan: 13%) were determined at temperatures of 90 and 100 °C. The corresponding steady-state values are 20.1 and 25.7%. As discussed in Section 3.1, at this potential the potentiodynamic data in the negative-going scan should be more affected by systematic distortions arising from the experiment (decay time of the CO_2 signal) than those in the positive-going scan. They are furthermore affected by the convolution of potential effects and time effects, and we would expect a lower adsorbate coverage in the negative-going scan than under steady-state conditions. For the positive-going scan, this should be opposite. The influence of the varying adsorbate coverage is illustrated also in the temporal evolution of the Faradaic and CO_2 ion current transients before reaching steady-state conditions.

Going to lower potentials, the differences between CO_2 current efficiencies determined under steady-state conditions in the potentiostatic measurements and those derived from potentiodynamic measurements become even more pronounced. For instance, values of 24% (positive-going scan, negative going scan: 31%) and 34% (positive-going scan, negative-going scan: 42%) were calculated at 0.48 V for 90 and 100 °C in the potentiodynamic measurements, compared to 36.5% and 45% under steady-state conditions. At this potential, not only effects arising from the convolution of potential and time effects (different adlayer coverage and composition in the potentiodynamic measurements) play a role, but also effects arising from the oxidation of adsorbates pre-formed at lower coverages (positive-going scan) and from distortions in the measured CO_2 ion currents (negative-going scan) as discussed before in Section 3.1 contribute significantly.

These results essentially preclude the use of CO_2 current efficiency values calculated from potentiodynamic data for quantitative discussions, and limit them to qualitative estimates of the CO_2 current efficiency.

Similar to the potentiodynamic experiments in Section 3.1, we also evaluated the influence of the ethanol concentration on the ethanol oxidation activity and on the selectivity for complete oxidation to CO_2 under steady-state conditions, and similar potentiostatic measurements were performed in 0.01 M ethanol solution (Fig. 4). The resulting current–time profiles closely resemble those obtained in 0.1 M solution, with measurable ethanol oxidation currents and CO_2 signals at potentials of 0.48 V and above. Also in this case, the Faradaic current increases significantly when going to 0.58 and 0.68 V. For the latter potential, however, the increase is less pronounced than for 0.1 M ethanol solution. For the mass spectrometric CO_2 signals, the steady-state ion currents even decrease between 0.58 V and 0.68 V. The resulting current efficiencies for CO_2 formation, however, are generally higher than those measured in 0.1 M solution, yielding values between 87% (100 °C) and 5.1% (23 °C) at 0.48 V (see Table 1). Increasing the potential to 0.58 V,

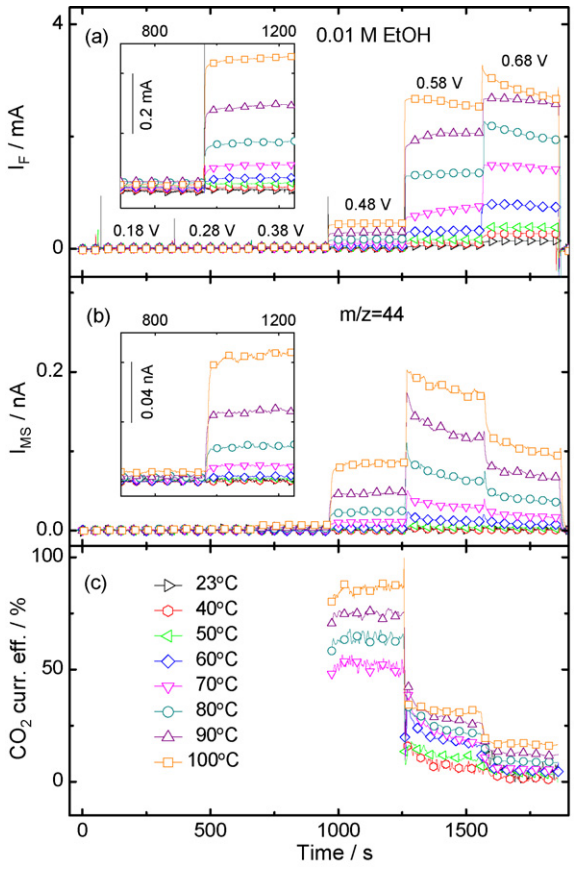

Fig. 4. Simultaneously recorded current transients of the Faradaic current (a) and the CO_2 ion currents for $m/z = 44$ (b), and the corresponding current efficiency for CO_2 formation (c) during potentiostatic oxidation of ethanol on a Pt/Vulcan catalyst in 0.01 M ethanol solution pressurized with 3 bar Ar overpressure at elevated temperatures (temperatures see figure). Catalyst loading 40 $\mu g_{Pt}\,cm^{-2}$, electrolyte flow rate 15 $\mu L\,s^{-1}$.

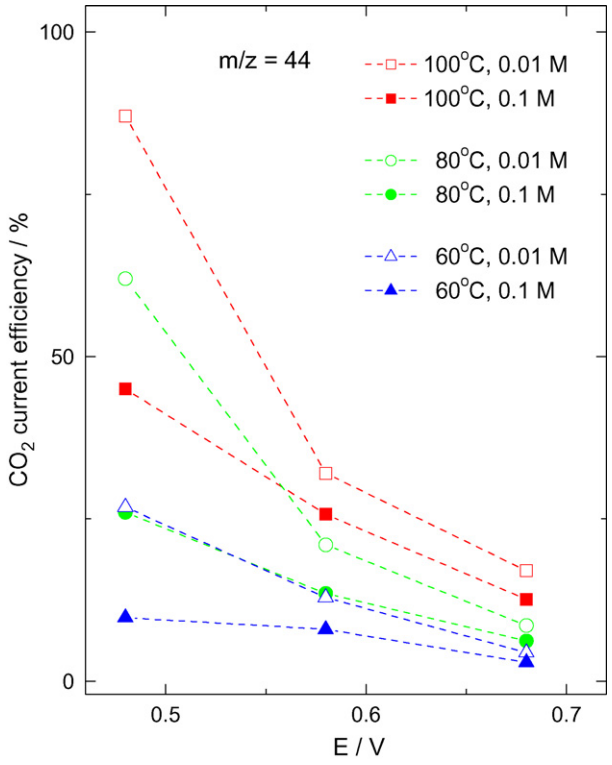

Fig. 5. Dependence of the steady-state current efficiency for CO_2 formation (potentiostatic measurements) on the variation of concentration at elevated temperatures and different potentials (see figure): 60 °C (triangles), 80 °C (circles) and 100 °C (rectangles).

the range of the CO_2 current efficiencies decreased to between 32% (100 °C) and 3.7% (23 °C), and also at 0.68 V they are considerably higher than those obtained in 0.1 M ethanol solution (see Table 1). The pronounced increase in CO_2 current efficiencies compared to 0.1 M ethanol solution clearly demonstrates that the CO_2 current efficiencies at a given temperature depend strongly on the ethanol concentration. The simultaneous influence of reaction temperature and ethanol concentration is illustrated in Fig. 5, where the CO_2 current efficiencies obtained at 60, 80 and 100 °C are plotted for both concentrations and at the three potentials 0.48, 0.58 and 0.68 V. At the same temperature, the CO_2 current efficiency increases by a factor of 1.5 at 0.48 V and 100 °C upon decreasing the concentration from 0.1 to 0.01 M. On the other hand, increasing the temperature from 80 to 100 °C at the same concentration (0.01 M) and electrode potential (0.48 V), the CO_2 current efficiency increased by about a factor of 1.4 (for a more extensive discussion see following section).

The present observation of slowly increasing CO_2 current efficiencies at temperatures up to 60 °C differs from our findings in an earlier DEMS study on ethanol oxidation on the same Pt/C catalyst, where the CO_2 current efficiency was found to decrease with temperature [10]. A similar discrepancy appears also between a previous DEMS study on methanol oxidation [54] and recent high-temperature/high-pressure measurements in our laboratory [38,55]. We explain this discrepancy in trends – the absolute values of the CO_2 current efficiency are low in this temperature range in both EOR studies – by modifications of the CO_2 permeation behavior through the porous membrane used in these lower temperature DEMS studies [10,54], which reduce the CO_2 transport in the presence of methanol or ethanol compared to the calibration measurements, where these species are not present. Such effects are absent in the non-porous membrane used in the high-temperature/high-pressure measurements. These experimental effects will be corroborated and discussed in more detail in a forthcoming publication.

Similar observations of an increasing CO_2 current efficiency with higher temperatures were reported also for ethanol oxidation on a Pt or PtRu catalyst MEA in a DEFC by Aricó et al. [19] and by Rao et al. [20]. The former authors reported a high CO_2 current efficiency of 95% for measurements in a DEFC (PtRu anode catalyst) at 145 °C [19]. In the latter work, CO_2 current efficiencies of up to 75% were obtained at 0.6 V and 90 °C in 0.1 M ethanol solution on a Pt/C catalyst MEA (slightly lower values at 0.5 and 0.7 V). Interestingly, very low values <5% were given, for PtRu catalysts. Furthermore, the CO_2 formation current efficiency was found to increase with catalyst loading, to decrease with increasing flow rate and also with ethanol concentration [20]. From the product yields reported by Rousseau et al. [6], who investigated ethanol oxidation in a 2 M ethanol operated DEFC with a Pt/C anode, one can calculate CO_2 current efficiencies of 35% for reaction at 80 °C (60% Pt/C catalyst, cell voltage 0.3 V equivalent to an anode potential voltage of ~0.55 V), which agrees qualitatively with the results by Rao et al., considering the much higher ethanol concentration. In contrast, Wang et al determined acetaldehyde as main reaction product for reaction at 190 °C in a DEFC operated by a highly concentrated ethanol solution (76% for an ethanol: water ratio of 1:2), with increasing water content the amount of CO_2 increased [9]. Higher CO_2 current efficiencies for decreasing ethanol concentrations were obtained also in model studies on ethanol oxidation over massive Pt electrodes [21,53] and over Pt/C catalyst thin-film electrodes [10].

The experimental findings in the above studies and in the present work can be summarized in the following correlations:

The current efficiency for CO_2 formation increases with

increasing catalyst loading [10,20],
decreasing electrolyte flow rate (decreasing mass transport) [20],
decreasing ethanol concentration [10,20,21,53],
decreasing electrode potential [20,21],
higher reaction temperature [19,20].

The first three findings can be explained by transport effects, which are well known in Heterogeneous Catalysis, where in reactions with different products a lower space velocity is known to drive the product distribution towards their equilibrium composition [56]. In a microscopic picture, the increasing catalyst loading/decreasing electrolyte flow/decreasing ethanol concentration increase the probability that volatile incomplete oxidation products, in the present case mainly acetaldehyde, can re-adsorb and react further to CO_2 before leaving the catalyst bed ('desorption–re-adsorption–further reaction' concept), as described in detail in ref. [57], and proposed already earlier for methanol oxidation [58]. These 're-adsorption–further reaction' effects in fact become dominant under integral reaction conditions in a realistic fuel cell.

Specifically for ethanol oxidation, another effect may lead to decreasing CO_2 current efficiencies at higher ethanol concentrations. Reaction between acetaldehyde and ethanol may result in ethanal diethylacetal formation, which indeed was detected in the exhaust of a DEFC operated with pure ethanol [9]. This way, further reaction of acetaldehyde to CO_2 is inhibited, and the CO_2 current efficiency is reduced accordingly. With decreasing ethanol concentration (higher water-to-ethanol ratio), the yields of ethanal diethylacetal were found to decrease in that study, due to hydrolysis of ethanal diethylacetal to the initial reactants ethanol and acetaldehyde, and thus in an increasing CO_2 yield [9].

Furthermore, in dilute aqueous solutions, acetaldehyde is hydrated to the corresponding gem-diol [59,60], which in turn may decompose to CO_2 upon adsorption. Since in this case there is no additional oxygen required for CO_2 formation, this can lead to CO_2 formation even at low potentials, where water splitting is inhibited [61]. Similar effects were observed and discussed also for the adsorption/oxidation of formaldehyde [62–64]. Since acetaldehyde is formed as one of the two incomplete oxidation products during ethanol oxidation, its decomposition to CO_2 will also affect the CO_2 current efficiency and allow CO_2 formation even at potentials where water splitting and hence OH_{ad} formation are essentially inhibited [65].

While there is no doubt about the general occurrence of these latter processes, a quantitative assessment of their contributions under present reaction conditions is not yet possible and will require further work, focusing on the adsorption/reaction behavior of acetaldehyde. The separation of contributions arising from these processes from general transport effects as described above ('desorption–re-adsorption–further reaction' concept) is complicated also since they result in a similar trend, namely an increasing CO_2 current efficiency with decreasing ethanol concentration.

Further modifications of the CO_2 current efficiency measured in a fuel cell may arise from an inhomogeneous distribution of the potential (current) in a fuel cell MEA [66,67], which can result in different product distributions over the flow field, while at the exhaust only the average value is measured.

The decrease in CO_2 formation with increasing potential is generally attributed to the decreasing tendency for C—C bond breaking with higher potential [47–50] and to the increasing coverages of OH_{ad}/surface oxide species at higher potentials, which reduces the number of pairs of vacant surface sites required for C–C bond breaking (see also the discussion in the next section).

Finally, the increasing CO_2 current efficiency with higher temperature, which reflects a more pronounced temperature dependence and hence a higher activation barrier for CO_2 formation than for the overall ethanol oxidation process, will be discussed in the next section.

3.3. Apparent activation energies

The temperature dependent steady-state values of the Faradaic currents and the CO_2 ion currents (after normalization to a common K^*_{44} value, see Section 2.2) were used to calculate the apparent activation energies E_a for the overall oxidation of ethanol (Faradaic current) and for the complete oxidation of ethanol to CO_2 over the Pt/Vulcan catalyst at different reaction potentials. As evident from the Arrhenius plots in Fig. 6, the logarithmic oxidation rates decrease linearly with $1/T$, indicating that there is no change in the rate determining step in the entire temperature range covered (23–100 °C). From the slopes of the Arrhenius plots, we calculate activation energies of 42 ± 2, 41 ± 2, and 40 ± 2 kJ mol^{-1} at poten-

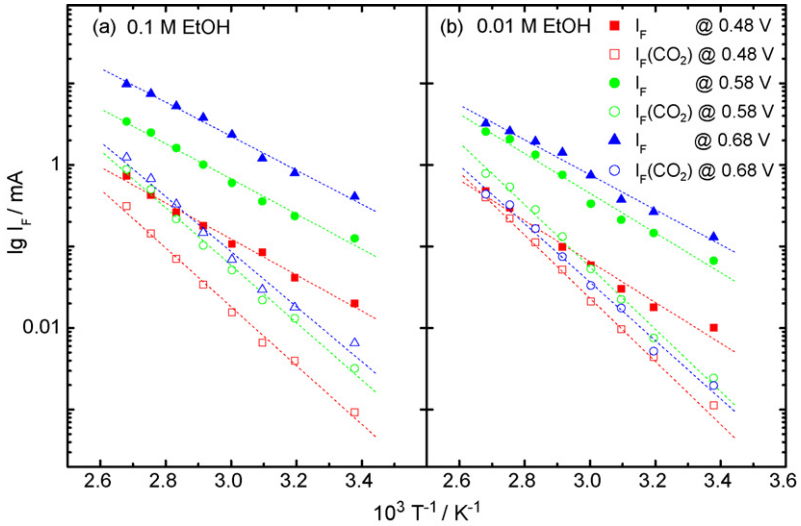

Fig. 6. Arrhenius plots of the overall ethanol oxidation rate (Faradaic current) and of the complete oxidation of ethanol to CO_2 (partial current for CO_2 formation) in 0.1 M ethanol solution (a) and 0.01 M ethanol solution (b) at different potentials (for potentials see figure). Electrolyte flow rate: 15 μL s^{-1}; catalyst loading 40 μg$_{Pt}$ cm^{-2}.

Table 2
Apparent activation energies for the overall ethanol oxidation reaction (Faradaic current) and complete oxidation to CO_2 (CO_2 partial reaction current) at different ethanol concentrations and potentials, determined from steady-state reaction currents (see Fig. 6).

E/V	0.1 M Ethanol		0.01 M Ethanol	
	E_a/kJ mol^{-1}	$E_a(CO_2)$/kJ mol^{-1}	E_a/kJ mol^{-1}	$E_a(CO_2)$/kJ mol^{-1}
0.48	42 ± 2	68 ± 2	48 ± 3	74 ± 3
0.58	41 ± 2	67 ± 2	46 ± 3	73 ± 3
0.68	40 ± 2	65 ± 3	41 ± 2	69 ± 3

tials of 0.48, 0.58 and 0.68 V, respectively, for the overall ethanol oxidation reaction in 0.1 M ethanol solution. The corresponding activation energies for complete oxidation to CO_2 are 68 ± 2, 67 ± 2, and 65 ± 3 kJ mol^{-1}, respectively (see Table 2). The apparent activation energy for the lower ethanol concentration (0.01 M) are 48 ± 3, 46 ± 3, and 41 ± 2 kJ mol^{-1} for the overall ethanol oxidation reaction and 74 ± 3, 73 ± 1, and 69 ± 3 kJ mol^{-1} for complete oxidation to CO_2. The similarity of the corresponding apparent activation energies for 0.1 and 0.01 M ethanol solution and for the different potentials as well as the fact that the logarithmic rates lie on a straight line over the entire temperature range in the Arrhenius plots indicate that (i) the apparent activation barriers measured in the two reaction pathways, respectively, can be associated with a single reaction step, at least for complete oxidation to CO_2 (see also below), and that (ii) the rate limiting steps are the same over the entire temperature and ethanol concentration range covered in the present study, but change with potential.

Our values of the apparent activation energy are significantly higher than those determined in previous fuel cell studies. Colmati et al. reported values of around 26 kJ mol^{-1} for the apparent activation energy, determined from the (steady-state) Faradaic current in a 1 M ethanol feed operated DEFC over a commercial Pt/C catalyst (20 wt.%) anode in the temperature range 70–100 °C (cell potential 0.3 and 0.4 V, equivalent to an anode potential of 0.45 and 0.55 V, respectively) [68]. For PtRu/C catalysts, the corresponding value was ~32 kJ mol^{-1} in the same potential regime. Rao et al. obtained values of 31 kJ mol^{-1} for the overall reaction and 53 kJ mol^{-1} for complete oxidation to CO_2 at 0.6 V in measurements on a Pt/C catalyst MEA with a 40% Pt/C catalyst (0.1 M ethanol, temperature range 30–90 °C) [20]. The activation energy for complete oxidation to CO_2 was calculated using mass spectrometric data after correcting the m/z = 22 (CO_2^{2+}) ion current for temperature effects. Comparison with the results of a previous model study [10], which covered reaction temperatures up to 60 °C, is hardly possible, since in that study the activation energies were determined from potentiodynamic data, which as discussed above may result in considerable deviations from the steady-state situation.

The trend of a decreasing apparent activation barrier for the overall ethanol oxidation reaction upon going to higher ethanol concentrations, from 32 kJ mol^{-1} in 0.1 M ethanol solution [20] to 26 kJ mol^{-1} in 1 M ethanol feed [68], agrees with the findings in our study, where the value decreased from 46 ± 3 to 41 ± 2 kJ mol^{-1} for changing from 0.01 to 0.1 M ethanol solution, and accordingly we expect the apparent activation energy to further decrease when going to even higher concentrations (1 M). The absolute values for the activation energies for the overall ethanol oxidation reaction, however, are significantly lower in the above studies than the values measured under comparable temperature and at similar potential in the present work (41 ± 2 kJ mol^{-1} at 0.58 V in 0.1 M ethanol solution). Main reasons for this discrepancy are (i) that the ethanol oxidation reaction proceeds via a complex network of individual reactions, where the Faradaic current only probes the sum of all partial reaction currents, and (ii) the different mass transport conditions in model studies and in a real fuel cell. Differences in the contributions from the various reaction pathways, which are likely to have different activation energies, will result in varying values of the apparent activation energy. The existence of some differences in the contributions from different pathways is illustrated by the still higher CO_2 current efficiencies obtained in the fuel cell measurements at similar temperature and anode potential (see discussion in the previous section) compared to our results. In summary, although we can not quantitatively explain the differences between the apparent activation energies for the ethanol oxidation reaction measured in fuel cell studies and in our model study at similar potential and temperatures, they can be understood on a qualitative basis.

The higher value of the apparent activation energy for complete oxidation of ethanol to CO_2 compared to the overall oxidation reaction is mainly attributed to a higher barrier for C—C bond breaking compared to oxidation of the C-OH group. This reaction step is not required for partial oxidation of ethanol to acetaldehyde and acetic acid, which at lower temperatures dominates the overall ethanol oxidation reaction and which only includes C-OH oxidation and water splitting (OH_{ad} formation) as activated steps. Considering that with increasing temperature the complete oxidation to CO_2 contributes increasingly more to the overall reaction and that the effects on the ethanol oxidation current are even higher due to the higher number of electrons released during complete oxidation to CO_2 (12 electrons per ethanol molecule) than during partial oxidation to acetaldehyde (2 electrons per ethanol molecule) or to acetic acid (4 electrons per ethanol molecule), the barrier for the rate limiting step in the oxidation of the C–OH group must be even lower than the measured barrier of the overall ethanol oxidation reaction. Effects caused by the temperature dependent surface blocking by strongly adsorbed reaction intermediates/side products, mainly by CO_{ad}, should at least to zeroth order affect both reaction pathways, incomplete oxidation to acetaldehyde/acetic acid and complete oxidation to CO_2, in the same way. In a more detailed perspective, different site requirements may result in different site blocking effects for the two different pathways, which may result in slightly different effects for the two pathways.

In order to further elucidate the influence of C–C bond breaking, one may compare the present results with previous data on methanol oxidation. Wakabayashi et al. determined activation energies between 15 and 24 kJ mol^{-1} in potentiodynamic measurements in a thin-layer flow cell for potentials between 0.6 and 0.7 V on a Pt electrode (temperature range 20–120 °C) [29]. On the other hand, Madden et al. reported activation energies of around 70 kJ mol^{-1} at 0.35 V in a flow cell in potentiostatic measurements [30], and recent high-temperature DEMS measurements in our laboratory performed on the same catalyst and at the same experimental conditions as used in the present study led to activation energies of 58 ± 3 kJ mol^{-1}, and 64 ± 3 kJ mol^{-1} for the overall methanol oxidation reaction and for complete methanol oxidation to CO_2, respectively, at 0.6 V (potentiostatic measurements) [38,55]. The differences between these values are mainly attributed to differences between potentiodynamic [29] and potentiostatic [30,55] measurements under steady-state conditions, additional effects arise from the differences in potential, electrolyte flow and electrolyte concentration. The rather similar values for the activation energies for complete oxidation to CO_2 of methanol and ethanol (67 ± 2 kJ mol^{-1}) under these conditions may indicate that in both cases the same reaction step, e.g., CO_{ad} oxidation is rate limiting for this process. At higher potentials, CO_2 formation from ethanol will be limited by C–C bond breaking [47–50]. This interpretation is supported also by results of a recent HT/HP DEMS study on the electrooxidation of ethylene glycol over the same Pt/C catalyst, where similar trends were observed as in the present study [69].

C—C bond breaking has two effects: it provides $C_{1,ad}$ species which are required for the further oxidation to CO_2 (positive effect

on the reaction), but the same species may block also the surface for further reaction (negative effect on the reaction). Only if the removal of these species is not rate limiting, a further increase of the C—C bond breaking rate will lead to an overall improvement of the reaction kinetics, i.e., a higher ethanol oxidation current. Otherwise, the increasing steady-state coverage of CO_{ad} and $CH_{x,ad}$ species may result in a decrease of the ethanol oxidation current due to a decreasing partial oxidation of ethanol. For very low rates of CO_{ad} oxidation, also slow formation of these species is required to keep the steady-state coverage of these species at a level which still allows partial oxidation of ethanol (enough vacant surface sites for reaction). In that sense, catalysts with an improved activity for C—C bond breaking are not beneficial for the ethanol oxidation reaction, unless they are also more active for oxidation of adsorbed CO_{ad} and $CH_{x,ad}$ species.

For technical applications finally it is important to note that increasing reaction temperatures not only result in a higher reaction rate, but, due to the higher activation barrier for complete oxidation of ethanol to CO_2 compared to its partial oxidation, also in decreasing amounts of acetaldehyde and acetic acid formation. Extrapolating the data in Fig. 6 to higher temperatures, one can estimate that under current reaction conditions and at 0.48 V complete conversion to CO_2 will be reached at ~140 °C (0.1 M solution), provided there is no change in the reaction mechanism and rate determining pathways. For higher potentials, this temperature will shift to higher values (175 °C at 0.58 V).

4. Conclusions

Potentiodynamic and potentiostatic DEMS measurements of the ethanol oxidation reaction on carbon supported Pt/Vulcan thin-film catalyst electrodes performed under fuel cell relevant but nevertheless well defined reaction and transport conditions (controlled electrolyte transport, continuous reaction, elevated temperatures and pressure) and on relevant materials (supported catalysts, 100% catalyst utilization), led to the following conclusions:

1. Both the overall reaction rate, as measured by the Faradaic current, and the rate for CO_2 formation increase significantly with increasing reaction temperature. The increase with temperature is much more pronounced for complete oxidation to CO_2 than for the overall ethanol oxidation reaction. Accordingly, the apparent activation energies are significantly higher for CO_2 formation than for the overall reaction (68 ± 2 kJ mol^{-1} vs. 42 ± 2 kJ mol^{-1} in 0.1 M ethanol solution, 0.48 V).
2. In the same way, also the current efficiency for CO_2 formation increases significantly with temperature, in particular at temperatures >60 °C, from negligible CO_2 formation at room temperature (4.6% under steady-state conditions, 0.48 V) to 45% at 100 °C. Accordingly, the formation of incomplete oxidation products (C_2 by-products), which is dominant at ambient temperature, decreases significantly with temperature. High current efficiency values for CO_2 formation over the Pt/C catalyst can be reached, however, only at low potentials (0.38 and 0.48 V) and hence at rather low current densities (geometric surface area normalized current density): 23% at 0.4 mA cm^{-2} (0.38 V, 0.1 M ethanol solution), 45% at 3.7 mA cm^{-2} (0.48 V, 0.1 M ethanol solution), and 87% at 2.3 mA cm^{-2} (0.48 V, 0.01 M ethanol solution) (all at 100 °C).
3. The activation energies decrease slightly with potential, from 42 ± 2 and 68 ± 2 kJ mol^{-1} at 0.48 V to 40 ± 2 and 65 ± 3 kJ mol^{-1} at 0.68 V in 0.1 M solution for the overall reaction and the pathway for CO_2 formation, respectively. Correspondingly, also the current efficiencies for CO_2 formation decrease with increasing potential, e.g., from 45% (14.8%) at 0.48 V to 12.6% (3.9%) at 0.68 V at 100 °C (70 °C). The decrease in both quantities with potential is associated with the transition from rate limiting CO_{ad} oxidation at lower potentials to rate limiting C–C bond breaking (CO_{ad} formation) at higher potential (see point 2).
4. The current efficiency for CO_2 formation increases with decreasing ethanol concentration, e.g., from 48% in 0.1 M to 87% in 0.01 M ethanol solution (0.48 V, 100 °C). This increase in CO_2 formation is explained by transport effects, namely an increasing tendency for re- adsorption and further oxidation of incomplete oxidation products at lower concentrations. Similar effects are proposed also as origin for the increasing CO_2 current efficiency with increasing catalyst loading and decreasing electrolyte flow reported in the literature.
5. Significant differences between the CO_2 current efficiencies determined in potentiodynamic measurements and under steady-state conditions in potentiostatic measurements at similar potentials are explained by a combination of different effects specific for potentiodynamic measurements: (i) the convolution of potential and time effects in potentiodynamic measurements, which result in different adlayer coverages and compositions in both types of measurements; (ii) the oxidation of adsorbed species pre-formed at other (lower) potentials, which leads to lower electron yields per CO_2 molecule formation, and (iii) distortions in the CO_2 detection induced by the experiment. Due to these effects, only the CO_2 current efficiencies determined under steady-state conditions are reliable for quantitative considerations, while the use of values determined in potentiodynamic measurements is limited to qualitative discussions of the trends.
6. The increasing similarity between the signals in the positive-going and negative-going scans in potentiodynamic measurements with higher temperatures is attributed to increasing contributions from ethanol bulk oxidation (decreasing contributions from pre-formed adlayer oxidation) due to the rapidly increasing activity. Hence, with increasing temperatures the system increasingly approaches steady-state conditions during potentiodynamic measurements.
7. The effective overall reaction rates and the CO_2 formation rates measured between 60 and 100 °C in the present study quantitatively follow the trends determined in the lower temperature range between room temperature and 60 °C in this and earlier studies, as illustrated by the linear correlation between $\ln i$ and $1/T$ over the full temperature range in the Arrhenius plots. Therefore we conclude that the rate limiting reaction steps in the two reaction pathways do not change in the entire temperature scale. Extrapolating these data to higher temperatures leads to complete ethanol conversion to CO_2 in 0.1 M ethanol solution (100% CO_2 current efficiency) at ~140 °C under present reaction conditions (0.48 V).

Finally, the drastic temperature and concentration effects evident from the present study demonstrate the importance of fuel cell relevant reaction and mass transport conditions (continuous reaction, continuous electrolyte and elevated temperature/pressure) in model studies aiming at a proper description of the reaction kinetics and the reaction mechanism in a realistic fuel cell.

Acknowledgements

This work was supported by the Federal Ministry of Research and Technology (project 03SF0311C), by the Helmholtz Association (project VH-VI-139) and by the State Foundation of Baden-Württemberg within the Project 'Portable Mini-Fuel Cells' (grant no. MBZ 20).

References

[1] R. Dillon, S. Srinivasan, A.S. Arico, V. Antonucci, J. Power Sources 127 (2004) 112.
[2] B.C.H. Steele, A. Heinzel, Nature 414 (2001) 345.
[3] C. Lamy, A. Lima, V. Le Rhun, F. Delime, C. Coutanceau, J.-M. Léger, J. Power Sources 105 (2002) 283.
[4] C. Lamy, E.M. Belgsir, in: W. Vielstich, H.A. Gasteiger, A. Lamm (Eds.), Fundamentals and Survey of Systems, vol. 1, Wiley, Chichester, 2003 (Chapter 19).
[5] C. Lamy, S. Rousseau, E.M. Belgsir, C. Coutanceau, J.-M. Léger, Electrochim. Acta 49 (2004) 3901.
[6] S. Rousseau, C. Coutanceau, C. Lamy, J.-M. Léger, J. Power Sources 158 (2006) 18.
[7] G. Li, P.G. Pickup, J. Power Sources 161 (2006) 256.
[8] E. Antolini, J. Power Sources 170 (2007) 1.
[9] J. Wang, S. Wasmus, R.F. Savinell, J. Electrochem. Soc. 142 (1995) 4218.
[10] H. Wang, Z. Jusys, R.J. Behm, J. Phys. Chem. B 108 (2004) 19413.
[11] D.J. Tarnowski, C. Korzeniewski, J. Phys. Chem. B 101 (1997) 253.
[12] C. Lamy, E.M. Belgsir, J.-M. Léger, J. Appl. Electrochem. 31 (2001) 799.
[13] F. Vigier, C. Coutanceau, A. Perrard, E.M. Belgsir, C. Lamy, J. Appl. Electrochem. 34 (2004) 439.
[14] J. Mann, N. Yao, A.B. Bocarsly, Langmuir 22 (2006) 10432.
[15] F.C. Simoes, D.M. dos Anjos, F. Vigier, J.-M. Leger, F. Hahn, C. Coutanceau, E.R. Gonzalez, G. Tremiliosi-Filho, A.R. de Andrade, P. Olivi, K.B. Kokoh, J. Power Sources 167 (2007) 1.
[16] H. Wang, Z.-P. Liu, J. Phys. Chem. C 111 (2007) 12157.
[17] T. Iwasita, J. Braz. Chem. Soc. 13 (2002) 401.
[18] O.A. Petrii, in: W. Vielstich, H.A. Gasteiger, A. Lamm (Eds.), Electrocatalysis, vol. 2, Wiley, Chichester, 2003 (Chapter 45).
[19] A.S. Aricò, P. Creti, P.L. Antonucci, V. Antonucci, Electrochem. Sol. Lett. 1 (1998) 66.
[20] V. Rao, C. Cremers, U. Stimming, L. Cao, S. Sun, S. Yan, G. Sun, Q. Xin, J. Electrochem. Soc. 154 (2007) B1138.
[21] H. Hitmi, E.M. Belgsir, J.-M. Léger, C. Lamy, R.O. Lezna, Electrochim. Acta 39 (1994) 407.
[22] N. Fujiwara, K.A. Friedrich, U. Stimming, J. Electroanal. Chem. 472 (1999) 120.
[23] V.M. Schmidt, R. Ianniello, E. Pastor, S. Gonzalez, J. Phys. Chem. 100 (1996) 17901.
[24] L. Colmenares, H. Wang, Z. Jusys, L. Jiang, S. Yan, G.Q. Sun, R.J. Behm, Electrochim. Acta 52 (2006) 221.
[25] H. Wang, Z. Jusys, R.J. Behm, J. Power Sources 154 (2006) 351.
[26] Q. Wang, Q.G. Sun, L.H. Jiang, Q. Xin, S.G. Sun, Y.X. Jiang, S.P. Chen, Z. Juys, R.J. Behm, PCCP 9 (2007) 2686.
[27] J. McBreen, W.E. O'Grady, R. Richter, J. Electrochem. Soc. 131 (1984) 1215.
[28] H. Nonaka, Y. Matsumura, J. Electroanal. Chem. 520 (2002) 101.
[29] N. Wakabayashi, H. Uchida, M. Watanabe, Electrochem. Sol. Lett. 5 (2002) E62–E65.
[30] T.H. Madden, N. Arvindan, E.M. Stuve, J. Electrochem. Soc. 150 (2003) E1.
[31] T.H. Madden, E.M. Stuve, J. Electrochem. Soc. 150 (2003) E571.
[32] I. Homma, T. Toda, J. Electrochem. Soc. 150 (2003) A1689.
[33] N. Wakabayashi, M. Takeichi, M. Itagaki, H. Uchida, M. Watanabe, J. Electroanal. Chem. 574 (2005) 339.
[34] J.L. Cohen, D.J. Volpe, H.D. Abruña, Phys. Chem. Chem. Phys. 9 (2007) 49.
[35] J. Fuhrmann, H. Zhao, E. Holzbecher, H. Langmach, M. Chojak, R. Halseid, Z. Jusys, R.J. Behm, Phys. Chem. Chem. Phys. 10 (2008) 3784.
[36] J. Otomo, S. Nishida, H. Takahashi, H. Nagamoto, J. Electroanal. Chem. 615 (2008) 84.
[37] J. Zhu, F. Cheng, Z. Tao, J. Chen, J. Phys. Chem. C 112 (2008) 6337.
[38] Z. Jusys, R.J. Behm, ECS Trans. 16 (2008) 1243.
[39] Z. Jusys, J. Kaiser, R.J. Behm, Phys. Chem. Chem. Phys. 3 (2001) 4650.
[40] T.J. Schmidt, H.A. Gasteiger, G.D. Stäb, P.M. Urban, D.M. Kolb, R.J. Behm, J. Electrochem. Soc. 145 (1998) 2354.
[41] H. Wang, Z. Jusys, R.J. Behm, Fuel Cells 4 (2004) 113.
[42] E. Herrero, B. Alvarez, J.M. Feliu, S. Blais, Z. Radovic-Hrapovic, G. Jerkiewicz, J. Electroanal. Chem. 567 (2004) 139.
[43] R.J. Behm, Z. Jusys, J. Power Sources 154 (2006) 327.
[44] H.A. Gasteiger, N. Markovic, P.N. Ross, E.J. Cairns, J. Electrochem. Soc. 141 (1994) 1795.
[45] D. Kardash, C. Korzeniewski, Langmuir 16 (2000) 8419.
[46] E.A. Batista, H. Hoster, T. Iwasita, J. Electroanal. Chem. 554–555 (2003) 265.
[47] S.-G. Sun, in: J. Lipkowski, P.N. Ross (Eds.), Electrocatalysis, Wiley-VCH, New York, 1998.
[48] Y.J. Fan, Z.Y. Zhou, C.H. Zhen, C.J. Fan, S.-G. Sun, Electrochim. Acta 49 (2004) 4659.
[49] M. Heinen, Z. Jusys, Y.-X. Chen, R.J. Behm, in preparation.
[50] S.C.S. Lai, S.E.F. Kleyn, V. Rosca, M.T.M. Koper, J. Phys. Chem. C 112 (2008) 19080.
[51] A. Ghumman, P.G. Pickup, J. Power Sources 179 (2008) 280.
[52] J. Shin, W.J. Tornquist, C. Korzeniewski, C.S. Hoaglund, Surf. Sci. 364 (1996) 122.
[53] G.A. Camara, T. Iwasita, J. Electroanal. Chem. 578 (2005) 315.
[54] H. Wang, H. Baltruschat, J. Phys. Chem. C 111 (2007) 7038.
[55] M. Chojak, Z. Jusys, R.J. Behm, in preparation.
[56] J.M. Thomas, W.J. Thomas, Principles and Practice of Heterogeneous Catalysis, VCH, Weinheim, 1997.
[57] Y.E. Seidel, A. Schneider, Z. Jusys, B. Wickman, B. Kasemo, R.J. Behm, Faraday Discuss. 140 (2008) 167.
[58] Z. Jusys, J. Kaiser, R.J. Behm, Langmuir 19 (2003) 6759.
[59] P. Greenzaid, Z. Luz, D. Samuel, J. Am. Chem. Soc. 89 (1967) 756.
[60] P. Greenzaid, Z. Luz, D. Samuel, J. Am. Chem. Soc. 89 (1967) 749.
[61] H. Wang, Z. Jusys, R.J. Behm, J. Appl. Electrochem. 36 (2006) 1187.
[62] E.A. Batista, G.R.P. Malpass, A.J. Motheo, T. Iwasita, J. Electroanal. Chem. 571 (2004) 273.
[63] M. Heinen, Z. Jusys, R.J. Behm, in: H.A. Gasteiger, W. Vielstich, H. Yokogawa (Eds.), Handbook of Fuel Cells, vol. 5, John Wiley and Sons, Chichester, 2009 (Chapter 11).
[64] Z. Jusys, R.J. Behm, in: M.T.M. Koper (Ed.), Fuel Cell Catalysis: A Surface Science Approach, John Wiley & Sons, Chichester, 2009 (Chapter 13).
[65] V. Climent, R. Gómez, J.M. Orts, J.M. Feliu, J. Phys. Chem. B 110 (2006) 11344.
[66] H. Ju, C.-Y. Wang, J. Electrochem. Soc. 151 (2004) A1954.
[67] M. Reum, S.A. Freunberger, A. Wokaun, F.N. Büchi, J. Electrochem. Soc. 156 (2009) B301.
[68] F. Colmati, E. Antolini, E.R. Gonzalez, J. Power Sources 157 (2006) 98.
[69] M. Chojak, Z. Jusys, R.J. Behm, submitted for publication.